NUMERICAL SIMULATION OF THERMAL-HYDROLOGICAL PROCESSES OBSERVED AT THE DRIFT-SCALE HEATER TEST AT YUCCA MOUNTAIN, NEVADA

Ronald T. Green[1] and Scott Painter[1]
[1])Center for Nuclear Waste Regulatory Analyses, U.S.A.

Abstract: Results from the four-year long heating phase of the Drift-Scale Heater Test at the Exploratory Studies Facility at Yucca Mountain, Nevada, provide a basis to evaluate conceptual and numerical models used to simulate thermal-hydrological coupled processes expected to occur at the proposed repository. A three-dimensional numerical model was built to perform the analyses. All model simulations were predicated on a dual (fracture and matrix) continuum conceptualization. A 20-percent reduction in the canister heat load to account for conduction and radiation heat loss through the bulkhead, a constant pressure boundary condition at the drift wall, and inclusion of the active fracture model to account for a reduction in the number of fractures that were hydraulically active provided the best agreement between model results and observed temperatures.

1. INTRODUCTION

Results from the Drift-Scale Heater Test (DST) at the Exploratory Studies Facility at Yucca Mountain (YM) were used to evaluate the capability of a multiphase code to simulate thermal-hydrological processes in partially saturated fractured rock. The DST is a planned eight-year long *in situ* heater test, with four years of heating followed by four years of cooling. The four-year heating phase was completed in January 2002. The test has been monitored using a vast array of instrumentation to measure, or infer, changes in temperature, saturation, stress, and chemistry.

For the modeling study presented in this paper, temperature and saturation distributions in the rock were simulated for the four-year heating phase of the DST. The model results were compared with measured temperatures and saturations at the onset of the test and with measured temperatures after three months, one year, and four years of heating to guide refinement of the model. These modeling studies are an important part of the process of assessing and developing confidence to independently evaluate the safety case for the proposed geologic repository at YM. The predictive modeling analyses reported in this paper were conducted as part of Task 2 of the DECOVALEX III program.

2. DRIFT-SCALE HEATER TEST DESCRIPTION

The DST is located in the Topopah Spring middle nonlithophysal (Tptpmn) unit, within the horizon of the proposed YM repository. The Tptpmn unit is approximately 30–40 m thick at the location of the DST, overlain by the Topopah Spring upper lithophysal (Tptpul) and underlain by the Topopah Spring lower lithophysal (Tptpll) units. The DST test block was characterized prior to the onset of heating. On-site characterization of the local geology and *in situ* hydrology was supplemented with laboratory tests of thermal-hydrological properties.

A plan-view schematic of the relative placement of the heated drift to the observation drift is shown in Figure 1. The 5-m diameter, 47.5-m long heated drift is closed at the east end by a thermal bulkhead. Approximately 12 m of the west end of the heated drift is lined with cast-in-place concrete ground support. Concrete inverts were placed along the entire floor of the heated drift to provide a flat surface. Thermal sources for the heated drift consist of nine canister heaters, placed end to end on the floor of the heated drift, and 50 wing heaters (25 on either side), emplaced in horizontal boreholes drilled into the sidewalls of the heated drift about 0.25 m below the springline. The wing heaters are spaced 1.83 m apart. Each wing heater has two segments, both 5 m long, separated by 1.67 m with a larger power output from the outer segment. The inner wing heater segment is separated from the heated drift wall by 1.5 m.

3. CONCEPTUAL MODEL

A three-dimensional numerical model was assembled to perform the analyses. A variably sized grid in the xz-plane, commonly referred to as an unstructured grid, was used to construct the numerical model. This allowed for higher resolution near the heated drift and the wing heaters, areas with

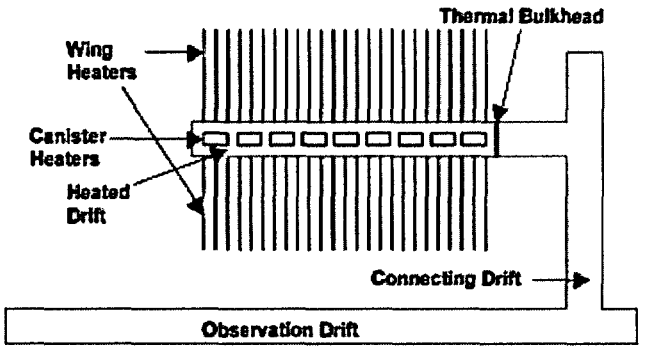

Figure 1. Plan-view schematic of the drift-scale heater test (DST).

the greatest gradients in temperature and saturation. The xz-plane was extruded as 14 planes in the y-direction to give the model its third dimension. Themedium was represented as a dual continuum, one for the matrix and one for the fractures. The fracture continuum implemented the active fracture model (Liu et al., 1998). Following are descriptions of these conceptualizations.

3.1 Dual continuum model

The dual continuum model (DCM) formulation is comparable to the dual permeability model (DKM) formulation (TRW Environmental Safety Systems, Inc., 2000). The DCM and DKM conceptualizations provide separate continua for the matrix and the fractures. The dual continua are coupled throughout the model domain by transfer functions for heat and mass transfer between the fractures and matrix. Use of a DCM increases the complexity of the numerical model used in the simulations, but offers the potential to realistically partition flow between matrix and fractures. Mass flow across the matrix/fracture interface is directionally dependent. When liquid pressure in the matrix exceeds the pressures in the fractures (i.e., $P_{lm} > P_{lf}$), liquid flow, Q_l, from the matrix to the fracture continuum is defined by

$$Q_l = \frac{A_{fm} A_{\mathrm{mod}}}{\mu_f} k_{harmonic} k_{rl,m\to f} \frac{P_{lm} - P_{lf}}{d} \qquad (1)$$

where the *m*, *f*, *l*, and *r* subscripts denote matrix, fracture, liquid, and relative. *d* is the distance from the matrix block center to the fracture center and $k_{harmonic}$ is the harmonic mean of the absolute permeability. A_{mod} is a modifier term included to allow a reduction, but not an increase, in the interfacial area between the matrix and fracture continua. For $P_{lf} > P_{lm}$, flow from the fractures to the matrix is defined by an equation analogous to Equation 1, with $k_{rl,m\to f}$ replaced by $k_{rl,f\to m}$. The matrix liquid-phase relative permeability is used for the matrix-to-fracture relative permeability $k_{rl,m\to f}$. For flow from fracture to matrix, a separate representation $k_{rl,f\to m}$ is used, thereby providing additional flexibility to the model. Similarly, an analogous form of Equation 1 defines mass flow of gas, Q_g, between matrix and fracture continua.

$$Q_g = \frac{A_{fm} A_{\mathrm{mod}}}{\mu_g} k_{harmonic} k_{rg} \frac{P_{gf} - P_{gm}}{d} \qquad (2)$$

The upstream value for the relative permeability is used to define gas flow between the matrix and fracture continua.

3.2 Active fracture model

The active fracture model for unsaturated flow through fractured rocks proposed by Liu et al. (1998) was used to modify flow through fractures. This model is based on the hypothesis that only a portion of connected fractures is active in conducting water. The hypothesis stipulates that: (i) all connected fractures are active if the system is fully saturated, (ii) all fractures are inactive if the system is at residual saturation, and (iii) the fraction of fractures that is active is related to water flux through the fractures. Liu et al. (1998) proposed that the fraction of active fractures be a power function of effective water saturation in connected fractures.

The liquid-phase relative permeability function for the fracture continuum defined in the Mualem relationship is modified to

$$k_{rl} = \left(S_l^{eff}\right)^{\frac{1+\gamma}{2}} \left\{1 - \left[1 - \left(S_l^{eff}\right)^{\frac{1+\gamma}{2}}\right]^m\right\}^2 \qquad (3)$$

to describe fracture to matrix flow. S^{eff} is effective saturation. Similarly, the van Genuchten relationship between effective saturation and capillary pressure is modified to

$$S_l^{eff} = \left[1 + \left(\alpha |P_c|\right)^{\frac{n}{1-\gamma}}\right]^{-m} \qquad (4)$$

where α is the inverse of the air-entry pressure, P_c is capillary pressure, n and m are fitting parameters,

and γ is a positive constant depending on the properties of the fracture network.

4. NUMERICAL SOLUTION

The multiphase simulator MULTIFLO was used to perform the thermal-hydrological simulations (Painter et al., 2001). MULTIFLO is based on a fully implicit formulation using a variable substitution approach. Space discretization is based on a block-centered grid using an integral finite-volume difference scheme, an approach suitable for an unstructured grid with arbitrary interblock grid connectivity and any polygon block boundary.

The numerical model grid is aligned with the axis of the heater drift. Vertical symmetry is assumed along and orthogonal to the drift axis. One plane of symmetry is placed mid-distance between the bulkhead and the terminus of the heated drift. The other plane is colinear with the drift axis. This allows modeling only ¼ of the DST block volume. The modeled area extends 200 m in the vertical direction and 100 m in the horizontal direction. The center of the heated drift is vertically placed at the midpoint of the model. Planes that intersect the heated drift have 1,123 nodes for each continuum. Planes that do not intersect the heated drift have additional nodes to account for the drift (i.e., 1175 nodes). The entire model, therefore, has 16,068 nodes in each continuum. Finer mesh resolution is included in areas expected to experience large temperature, saturation, and pressure gradients (Figure 2).

Three hydrostratigraphic units are included in the model: Tptpul (TSw33), Tptpmn (TSw34), and Tptpll (TSw35) of the Topopah Spring welded unit. Values for key properties assigned to the three units are presented in Table 1 (CRWMS M&O, 2001). Property values are assigned uniformly to each unit.

4.1 Boundary and Initial conditions

The vertical boundaries of the model were specified as adiabatic with no fluid flow. The top boundary was prescribed as a mixed boundary with specified flux and constant temperature and pressure. The bottom boundary was prescribed as a Dirichlet type with specified pressure, temperature, and gravity drainage. The mixed boundary condition at the top allows gas and heat transport in or out of the model while maintaining pressure and temperature as specified. The heater drift was not explicitly included in the model; instead, the heater drift wall was specified as constant pressure (at atmospheric), allowing for heat and mass loss out of the drift.

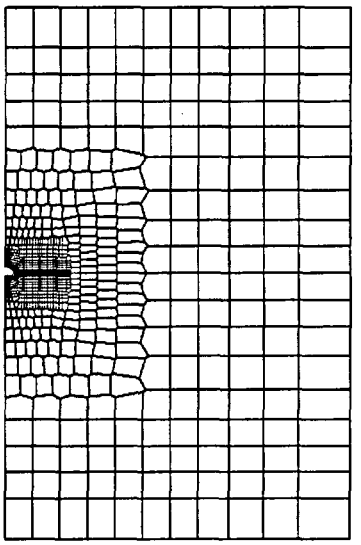

Figure 2. Unstructured grid assigned to the numerical model

Table 1. Key property values assigned to modeled units.

Unit	Tptpul	Tptpmn	Tptpll
Fracture permeability (m^2)	5.50e-13	2.76e-13	1.29e-12
Fracture porosity (-)	0.0066	0.010	0.011
Matrix Permeability (m^2)	3.08e-17	4.04e-18	3.04e-17
Matrix Porosity (-)	0.154	0.110	0.131
Thermal conductivity (dry)(W/m-K)	0.79	1.56	1.20
Thermal conductivity (wet)(W/m-K)	1.68	2.33	2.02

The temperature was specified as 22 and 26°C at the top and bottom model boundaries for a geothermal gradient of 0.02°C/m and a temperature of 24°C at the DST horizon. A static gas pressure difference of 2,156 Pa between the top and bottom

boundaries was specified to impose a gas gradient consistent with ambient conditions. Initial saturation was determined by simulating flow in the absence of heat at the DST for sufficiently long periods of time that steady-state flow conditions were approximated. An ambient matrix saturation of 0.92 in the TSw34 (Tptpmn) is predicted at an infiltration rate of 0.06 mm/yr. An infiltration rate of 0.3 mm/yr corresponds with an ambient matrix saturation of 0.99.

4.2 Model heat source

Heat was introduced into the model at the heated drift and at the inner and outer wing heaters. The heated drift cavity was not explicitly included in the model to avoid difficulties associated with representing the air space within the drift, radiative and convective heat transfer between the heater canisters and the drift wall, and the physics of heat and mass transfer at the drift-cavity/drift-wall boundary. The disadvantage to this simplification is that coupled thermal-hydrologic processes at the drift wall cannot be directly or easily investigated using this model.

The heat-source levels were applied uniformly to the drift boundary elements at the drift wall. The cylindrical wing heaters were represented as rectangular slabs, thereby smearing the heat deposition in the y-direction of the model. The DST experienced measured heat loads that deviated significantly (less) from the levels of the design heat loads since energized in December 1997. Piece-wise linear heat loads assigned to the model are compared with measured wing and canister heat loads in Figure 3. It was assumed that the decrease in cumulative heat load for the wing heaters occurred uniformly over both the inner and outer wing heaters. The canister heat load was reduced by 20 percent to account for heat loss through the thermal bulkhead.

5. MODEL RESULTS

Heat and mass transfer were simulated and compared to the DST data for the four-year heating phase of the DST. Temperature was directly measured throughout the DST affected volume. Saturation for the matrix is inferred using geophysical methods (i.e., electrical resistivity tomography, ground-penetrating radar, and neutron logging). Air permeability tests were conducted to provide a measure of fracture saturation. These measurements only provide a qualitative measure of

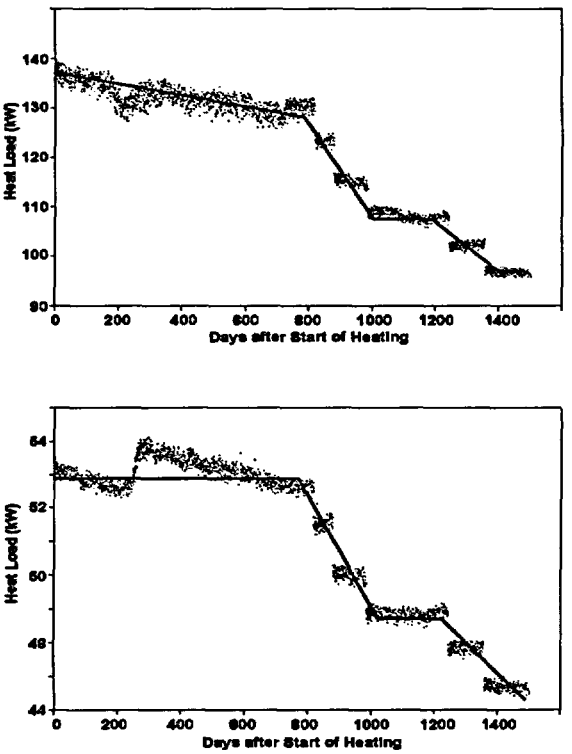

Figure 3. Measured (dots) and simulated (lines) heat load for the wing (top) and canister (bottom) heat sources.

saturation at the DST. Therefore, only temperature simulation results at this time, although inferred saturation measurement techniques may promote a clearer interpretation of the DST.

Temperatures calculated using a 2D model were measurements are used for comparison with compared with similar results using a 3D model to evaluate the effect of dimensionality. The comparison was made for the vertical plane located at the midpoint in the heated drift. The difference in temperatures calculated at the end of the four-year heating phase is illustrated in Figure 4. The 2D model calculated temperatures a maximum of 10.5 C higher at boiling isotherm located above the outer wing heater. Also calculated was a slight decrease in temperature in the halo formed just within the boiling isotherm. The slightly lower temperatures calculated in the 2D model are interpreted to be a consequence of increased condensed water caused by the slightly higher temperatures outside the boiling isotherm.

The effect of open versus closed drift-wall boundary conditions on calculated temperature was

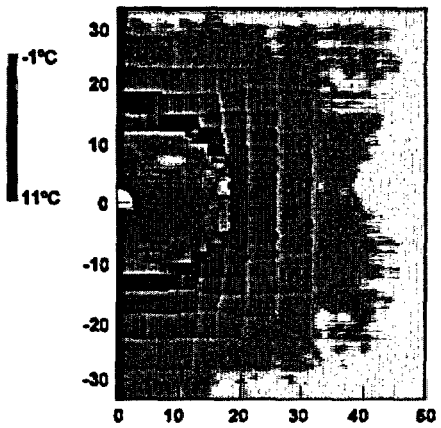

Figure 4. Temperature difference between 2D and 3D models after four years of heating.

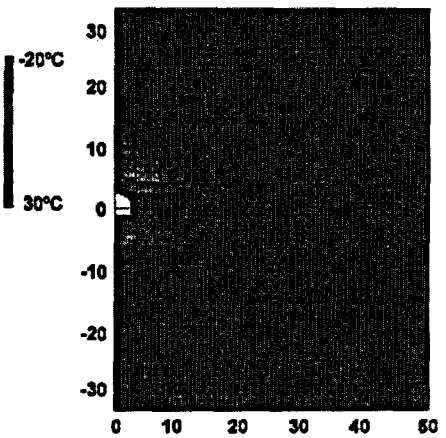

Figure 5. Temperature difference between open and closed boundary at the drift wall.

evaluated. Temperatures calculated for a model with the drift wall boundary treated as a Neumann boundary with no fluid and heat flow were compared with results from a model with a Dirichlet boundary condition at the drift wall. Temperature and saturation were allowed to vary while pressure was kept constant at one atmosphere at this boundary. The open boundary condition simulations resulted in reduced saturation at the drift wall. This lower saturation lowered the saturation-dependent thermal conductivity near the drift wall, resulting in higher temperatures in this region. As a consequence, temperatures calculated by the model with an open boundary at the drift wall were as much as 30°C higher near the drift and 20°C lower at the outer edge of the boiling isotherm (Figure 5). The open boundary at the drift wall is considered to more closely approximate the effects of heat and mass loss through the thermal bulkhead.

Matrix temperature, matrix saturation, and fracture saturation are calculated after four years of heating using the 3D model with dual continua, an active fracture model, and an open boundary at the drift wall (Figures 6-8). This model conceptualization provided the best agreement with temperatures measured during the DST at boreholes 158, 160, and162. Temperatures calculated for the fracture continuum are the same as those calculated for the matrix continuum. Maximum temperatures of 122, 185, and 275°C were calculated near the wing heaters after three months, one year, and four years of heating.

6. CONCLUSION

The multiphase code MULTIFLO was used to simulate the thermal-hydrological coupled processes observed during the four-year heating phase of the DST at Yucca Mountain, NV. The effects of different conceptual models on calculated temperature and saturation were compared. Conceptual models for the DST were evaluated by comparing simulated temperatures with temperatures measured at three boreholes. The models with the best agreement between calculated and measured temperatures included dual continua (matrix and fracture) and active fracture to reflect actual heat loads. The canister heat load was decreased by 20 percent to account for radiative and conductive heat loss through the thermal bulkhead.

The effect of dimensionality (i.e., 2D versus 3D) on temperature was evaluated. A maximum reduction in temperature of about 10°C near the wing heaters was calculated after four years of heating when a 3D model was used compared with a 2D model. Changing the drift wall from a closed boundary to an open boundary increased temperatures near the drift by a maximum of 30°C and decreased temperatures at the outer extent of the boiling isotherm by about20°C. Higher temperatures at the drift wall are attributed to lower thermal conductivities caused by drier rock.

The homogeneity of property assignment is reflected in the uniform nature of predicted matrix temperature and saturation. Saturation predicted for

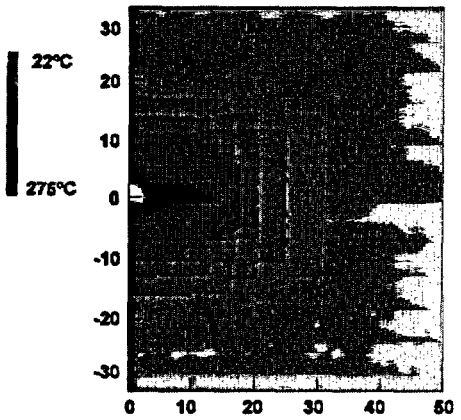

Figure 6. Calculated temperature after four years of heating.

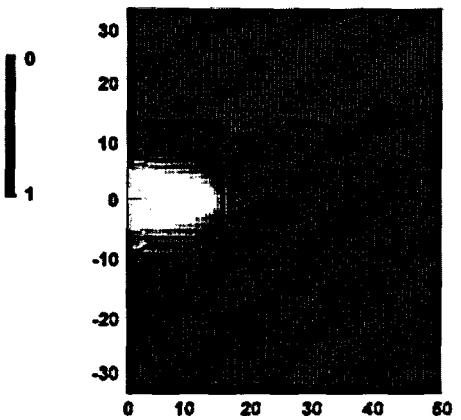

Figure 7. Calculated matrix saturation after four years of heating.

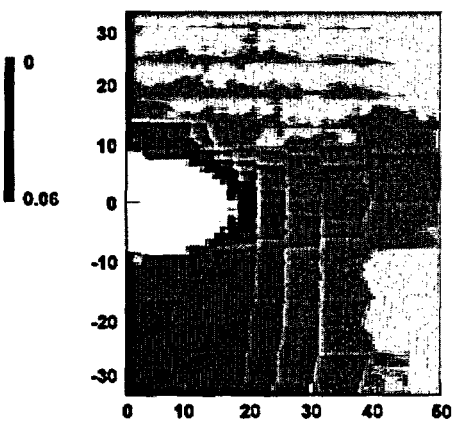

Figure 8. Calculated fracture saturation after four years of heating.

the fracture continuum indicated that water will build up in the areas above and outside of the boiling isotherm. Shedding of water off of the side of the boiling isotherm was observed. Saturation levels in the fracture continuum were highly sensitive to physical (i.e., porosity) and hydraulic (i.e., permeability) property values assigned to the fractures.

7. ACKNOWLEDGMENTS

This paper documents work performed by the Center for Nuclear Waste Regulatory Analyses (CNWRA) for the U.S. Nuclear Regulatory Commission (NRC). Activities reported here were performed on behalf of the NRC Office of Nuclear Material Safety and Safeguards, Division of Waste Management. The paper is an independent product of the CNWRA and does not necessarily reflect the views or regulatory position of the NRC.

REFERENCES

CRWMS M&O, *Multiscale Thermohydrologic Model, ANL-EBS-MD-000049, Revision 00, ICN02,* North Las Vegas, NV, Civilian Radioactive Waste Management System, Management and Operating Contractor, 2001.

Liu, H.H., C. Doughty, and G.S. Bodvarsson. *An active fracture model for unsaturated flow and transport in fractured rock.* Water Resources Research 34(10): 2,633–2,646. 1998.

Painter, S.L, P.C. Lichtner, and M.S. Seth. *MULTIFLO User's Manual MULTIFLO Version 1.5–Two-Phase Nonisothermal Coupled Thermal-Hydrologic-Chemical Flow Simulator.* Revision 3. Change 0. San Antonio, TX: Center for Nuclear Waste Regulatory Analyses. 2001.

TRW Environmental Safety Systems, Inc. *Thermal Tests Thermal-Hydrological Analyses/Model Report.* Las Vegas, NV: TRW Environmental Safety Systems, Inc. 2000.

THERMAL-MECHANICAL MODELING OF A LARGE-SCALE HEATER TEST

S.M. Hsiung[1], A.H. Chowdhury[1], and M.S. Nataraja[2]
[1]) Center for Nuclear Waste Regulatory Analyses, U.S.A.
[2]) U.S. Nuclear Regulatory Commission, U.S.A.

Abstract: Modeling of the drift-scale heater test at the Exploratory Studies Facility at Yucca Mountain, Nevada, U.S.A. was performed. The objectives of the analysis were to investigate the (i) temperature effects on mechanical deformation surrounding the heated drift and (ii) thermal-mechanical effects on rock-mass permeability. The continuum representation of a deformation-permeability relationship based on fracture normal stress was developed to assess rock-mass permeability variations because of temperature changes. The estimated rock-mass displacements and permeability variations as a function of heating time were compared with field measurements.

1. INTRODUCTION

DECOVALEX (acronym for the **DE**velopment of **CO**upled models and their **VAL**idation against **EX**periments in nuclear waste isolation) is an international cooperative project that has been designed to increase understanding of coupled thermal-hydrological-mechanical processes as they affect rock-mass responses and radionuclide release and transport from a repository to the biosphere. One of the tasks in Phase III of this cooperative project was modeling of the drift-scale heater test at the Exploratory Studies Facility at Yucca Mountain, Nevada, U.S.A. This task involved modeling the thermal-hydrological-mechanical-chemical behavior of the drift-scale heater test. This paper presents the results on (i) temperature-induced rock-mass deformation surrounding the heated drift and (ii) thermal-mechanical effects on rock mass permeability and their comparison with the measured data.

2. MODELING APPROACH

2.1 Description of Drift-Scale Heater Test

The host rocks for the proposed repository at Yucca Mountain include Topopah Spring Upper Lithophysal (Tptpul), Topopah Spring Middle Nonlithophysal (Tptpmn), Topopah Spring Lower Lithophysal (Tptpll), and Topopah Spring Lower Nonlithophysal (Tptpln) units. The drift-scale heater test facility is located in the Tptpmn unit (CRWMS M&O, 1997). The Tptpmn unit is 30–40 m thick at the location of the drift-scale test area. This unit is overlain by the Tptpul and underlain by the Tptpll units. The heater drift is approximately 5 m in diameter and 47.5 m long, and its entrance is closed by a thermal bulkhead.

Thermal sources for the heated drift consisted of 9 canister heaters, placed end to end on the concrete inverts of the heated drift, and 50 wing heaters (25 on either side) placed in horizontal boreholes drilled into the sidewalls of the heated drift approximately 0.25 m below the springline. The wing heaters were spaced 1.83 m apart and separated from the heater drift by 1.5 m.

2.2 Numerical Model

The analyses were conducted using a continuum approach using the FLAC computer code (Itasca Consulting Group, Inc., 2000). A two-dimensional vertical cross section was configured for numerical analysis. This cross section intersected the axis of the heated drift at middistance between the thermal bulkhead and its terminus. The FLAC models had a dimension of 1,000 m in width and 740 m in height, with the origin of the coordinates located at the center of the heated drift. A 5-m diameter circular drift was located with its center 500 m from the left boundary and 500 m from the bottom of the model domain.

Table 1. Rock-mass mechanical properties.

Unit	RMQ*	Young's modulus, GPa	Poisson's Ratio	Bulk Density, kg/m^3
Tptpul	2	14.28	0.23	2,160
Tptpmn	2	12.02	0.21	2,250
Tptpll	2	12.02	0.21	2,250

* Rock-Mass Quality

Fixed horizontal displacement boundaries were applied to the sides and a fixed vertical displacement boundary to the bottom of the model. The top of the model coincided with the ground surface.

Initial stresses consistent with overburden depth were applied as initial *in-situ* conditions.

The FLAC models included three thermal-mechanical lithologic units: Tptpul unit on the top, Tptpmn unit in the middle, and Tptpll unit on the bottom. The Tptpmn unit was 36 m thick, and its bottom was at 482 m from the bottom of the model domain. Note that the heater drift was located in the midheight of the Tptpmn unit.

The rock-mass mechanical and strength properties used for the three units were obtained from a CRWMS M&O report (CRWMS M&O, 1999) provided by the technical monitoring team and are listed in Tables 1 and 2. The acronym RMQ in Tables 1 and 2 means Rock-Mass Quality. The dilation angle for each unit was taken as half the corresponding friction angle. The rock-mass friction angle for the Tptpmn unit provided in CRWMS M&O (1999) was greater than the intact rock friction angle. The intact-rock friction angle was used in the analysis instead of the rock-mass value for the Tptpmn unit. To study the sensitivity of rock-mass properties on the thermal-mechanical effects, two variations of rock-mass properties also were modeled for each rock unit (Tables 3 and 4).

Table 2. Rock-mass strength properties.

Unit	RMQ	Cohesion, MPa	Tensile Strength, MPa	Friction Angle, Degree
Tptpul	2	1.4	1.13	46.00
Tptpmn	2	2.3	1.36	48.15
Tptpll	2	1.4	1.13	46.00

Table 3. Rock-mass mechanical properties for sensitivity analyses.

Unit	RMQ	Young's modulus, GPa	Poisson's Ratio	Bulk Density, kg/m^3
Tptpul	1	9.03	0.23	2,160
	5	20.36	0.23	2,160
Tptpmn	1	8.98	0.21	2,250
	5	24.71	0.21	2,250
Tptpll	1	8.98	0.21	2,250
	5	24.71	0.21	2,250

The measured temperature data were obtained from the technical monitoring team. These data were presented in three-dimensional grids in a two-day interval. Data selected as input for analyses were at 3, 6, and 9 months and 1, 2, 3, and 4 years of heating, and at the cross section 23 m from the thermal bulkhead. A temperature distribution in the rock mass after 4 years of heating is shown in Figure 1. When conducting the analyses, temperature changes between heating times were applied to simulate the heating process as a function of time. The thermal expansion coefficients, based on laboratory measurements (CRWMS M&O, 1999), for three rock units modeled are shown in Figure 2. It can be observed that the thermal expansion coefficients vary more than a factor of 5–7 from 25 to 300 °C. Two rock-mass failure criteria were used in the analyses to examine their effect on the rock-mass responses to the heating process: Mohr-Coulomb and ubiquitous failure criteria. When the ubiquitous failure criterion was used, fracture sets with dip angles (counterclockwise from the positive horizontal axis) of 82, 83.5, and 80.5 degrees were assumed for the Tptpul, Tptpmn, and Tptpll units, respectively (CRWMS M&O, 2000). The fracture cohesion, tensile strength, friction angle, and dilation angle were assumed to be 0.1 MPa, 0.0 MPa, 41 degrees, and 20.5 degrees for all three units (CRWMS M&O, 2000).

Table 4. Rock-mass strength properties for sensitivity analyses.

Unit	RMQ	Cohesion, MPa	Tensile Strength, MPa	Friction Angle, Degree
Tptpul	1	1.1	0.90	44.00
	5	2.9	2.26	47.00
Tptpmn	1	1.9	1.16	48.15
	5	3.9	2.22	48.15
Tptpll	1	1.1	0.90	44.00
	5	2.9	2.26	47.00

3. RESULTS AND DISCUSSIONS

3.1 Thermally Induced Rock-Mass Mechanical Responses

Thermally Induced Failure of Rock Mass

After heating started, the rock mass began to deform in response to the thermally induced stresses. At some point of heating, a yield zone developed for the models with the Mohr-Coulomb failure criterion in the Tptpul unit near the interface

between the Tptpul and Tptpmn units. This yield zone continued to grow upward throughout the heating process. The modeling results indicated that the timing of occurrence and the ultimate size of this yield zone were rock-mass property dependent. This yield zone tended to develop earlier and bigger for models using larger RMQ designations (e.g., RMQ 5 versus RMQ 2). The reason for this behavior is obvious because the differences between the Young's modulus among the RMQs are significant but the differences for the strength properties are relatively small. Thermally induced stresses are directly proportional to the Young's modulus. Consequently, it is more likely for the models with higher RMQ designations to develop yield zones larger than those with lower RMQ designations. Similar trend could be observed for development of a yield zone beneath the heated drift in the Tptpll unit at the interface between the Tptpmn and Tptpll units. This yield zone, however, developed later and relatively smaller in size than the yield zone above the heated drift [Figure 3(a)].

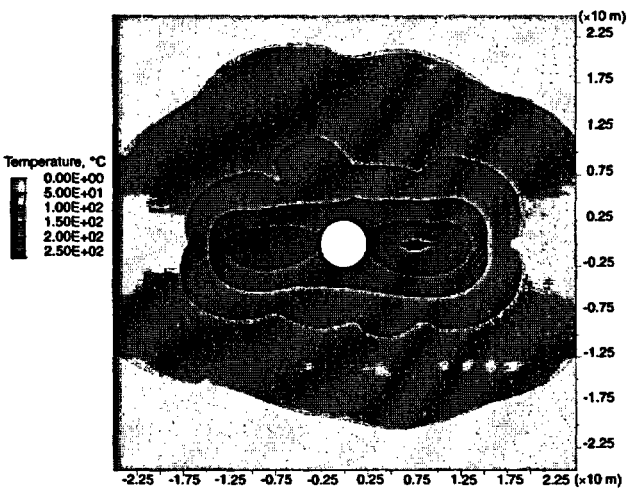

Figure 1. Temperature distribution in the rock mass after 4 years of heating.

The majority of rock yielding for models using the ubiquitous fracture failure criterion took place along fractures (fracture slip) because of fracture shear failure. As a result, the yielding behavior for the models using the ubiquitous failure criterion was substantially different from that for the models using the Mohr-Coulomb failure criterion. The fracture slip zones started first in the Tptpmn unit at the early stage of heating, mainly at a diagonal direction, forming an approximately 45-degree angle counterclockwise from the vertical axis and more than 50 degrees from the fracture dip angles [Figure 3(b)]. These fracture slip zones formed long shear bands stretching along the diagonal direction discussed earlier. As heating proceeded, new shear bands continued to develop vertically either upward or downward with respect to the heated drift. Also, these shear bands joined together. Another group of shear bands, at an approximately 45-degree angle clockwise from the vertical axis [Figure 3(b)], started to develop later and expand outward from the heated drift at a much slower rate than the shear bands at the perpendicular direction. Similar to the yielding trend observed for the models with the Mohr-Coulomb failure criterion, the shear bands tended to develop earlier and bigger for models using larger RMQ designations than those for models using smaller RMQ designations.

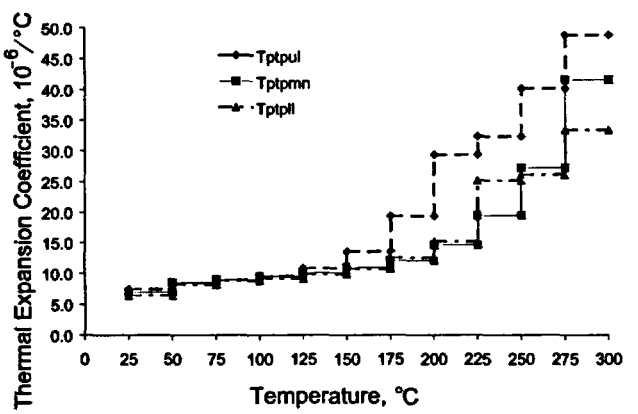

Figure 2. Thermal expansion coefficients of the three rock units.

Estimation of Rock-Mass Deformation

For comparison with measurements, rock-mass displacements from modeling results were estimated at the anchor locations of the four multiple-position extensometers (MPBXs) installed at the cross section approximately 21 m from the thermal bulkhead. For these four MPBXs, two were vertically oriented (one in the crown, MPBX9, and one in the invert, MPBX10). The remaining two (MPBX7 and MPBX8) were inclined at approximately 30 degrees to MPBX9 on either side of MPBX9. Figures 4, 5, 6, and 7 show the estimated displacements as a function of time for the model using the RMQ 2 rock-mass properties and the ubiquitous failure criterion. Note that each MPBX contained four anchors. Anchor 1 was located closest to the heated drift, while Anchor 4 was the farthest. Also included in the figures were the measured displacements. Letters E

and M in the legends denote the estimated results and the measured data.

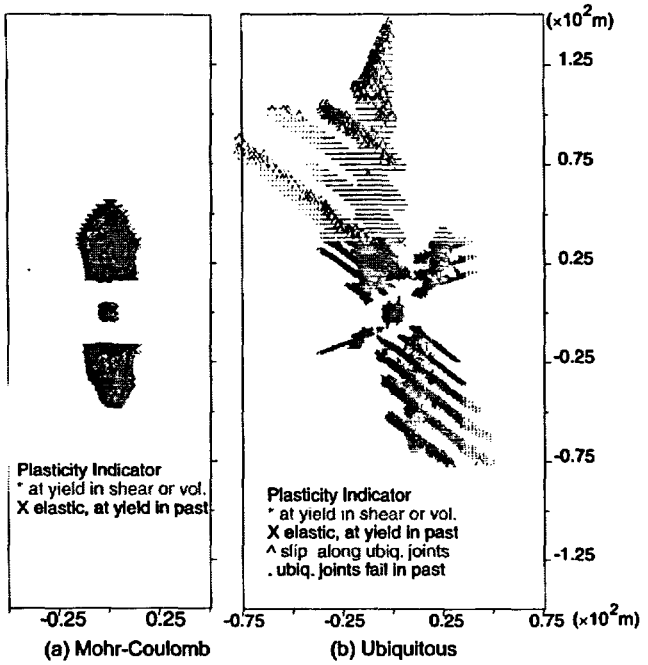

Figure 3. Thermally induced rock-mass yielding.

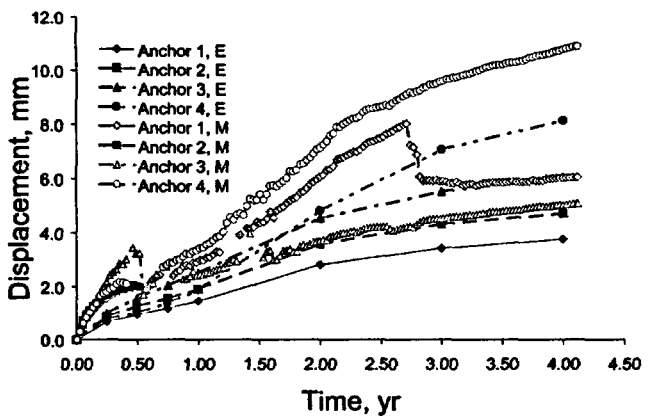

Figure 4. Anchor displacements for MPBX7.

Other than in the early stage of heating and regardless of the rock-mass properties or failure criteria used, the anchor displacements relative to the MPBX assembly head, located at the collar of the heated drift, were larger for the anchors located farther away from the heated drift. This displacement pattern indicated that the neighboring anchors of an MPBX continued to move away from each other as heating proceeded, suggesting an expansion of the rock mass between the two anchors. This behavior was not strictly observed in the measured data where some compression zones could be identified in the rock mass between anchors; for example, between Anchors 1 and 3 of MPBX7 (Figure 4) and between Anchors 2 and 3 of MPBX9 (Figure 6) and MPBX10 (Figure 7).

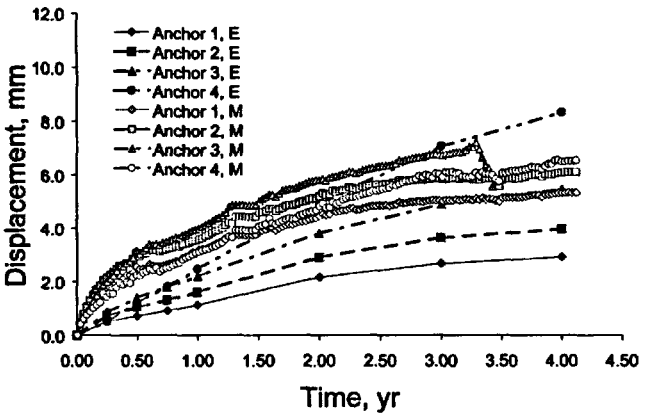

Figure 5. Anchor displacements for MPBX8.

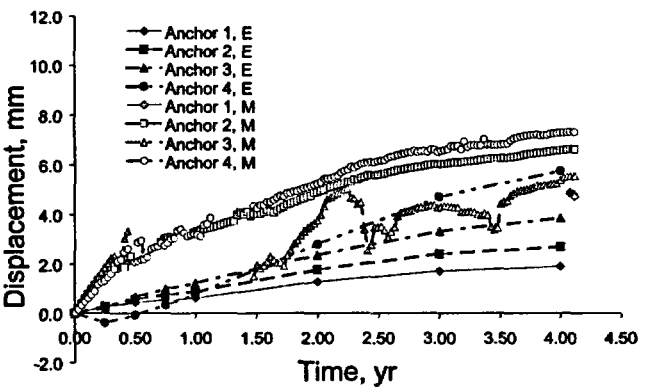

Figure 6. Anchor displacements for MPBX9.

In general, the estimated anchor displacements were larger when the rock-mass properties for larger RMQ designations were used. During the early stage of heating, Anchor 4 for both vertical MPBXs moved closer to the heated drift before Anchor 4 and the heated drift moved away from each other as heating proceeded further. This phenomenon was not observed in the measured data. Instead, the measured data indicated that all anchors in an MPBX had almost identical displacements for the first few months of heating, suggesting that only the rock mass between Anchor 1 and the assembly head deformed while there was not much deformation in the rock-mass between anchors.

The modeling results underestimated displacements for most anchors being evaluated. The measured anchor displacements for MPBX8 appeared similar in magnitude, suggesting that rock-mass expansion took place mostly in the

region between Anchor 1 and the assembly head, while the deformation between anchors was relatively small. This behavior might be a result of heterogeneity of the rock mass in the region not reflected in the modeling results.

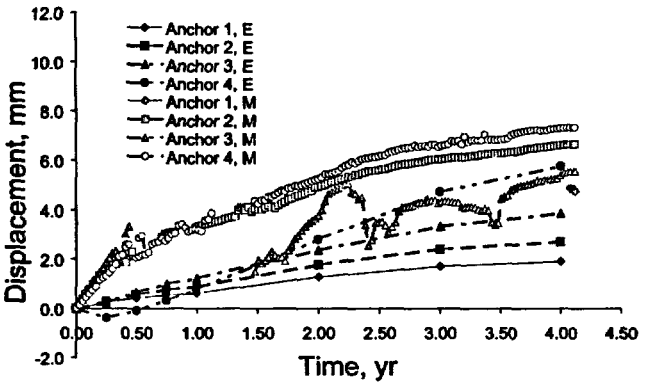

Figure 7. Anchor displacements for MPBX10.

The measured displacements also suggested potential localized fracture slip. For example, fracture slip in the rock mass between Anchors 2 and 3 of MPBX7 after approximately 6 months of heating caused Anchor 3 to move relatively closer to the assembly head. Another example was the slip of a fracture located possibly between Anchor 1 and the assembly head of MPBX7 at approximately 2.7 to 2.8 years of heating that caused Anchor 1 to move closer to the assembly head. These slips caused a displacement reduction. This distinct behavior represented one form of heterogeneity of the rock mass studied. A continuum analysis, such as that used in this study, could not capture this behavior. Consequently, the estimated displacement from modeling results would not be able to predict a displacement reduction representing fracture slip.

3.2 Thermal-Mechanical Effects on Rock-Mass Permeability

Permeabilities at Specified Locations

To assess the thermal-mechanical effects on rock-mass permeability, a deformation-permeability relationship based on fracture normal stress was developed.

$$k_f = k_{fr}\left(\frac{a}{c(\sigma_n+1)}\sqrt{\frac{\phi_{fr}}{12k_{fr}}}-\frac{e_{ftp}+e_{fsp}\tan\psi_f}{\phi_{fr}}\right)^3 \quad (1)$$

where k_f and k_{fr} are permeability at time of interest and reference permeability; a and c are constants, σ_n is the normal stress; ϕ_{fr} is the reference fracture porosity; e_{ftp} and e_{fsp} are rock-mass or fracture tensile and shear plastic strains; and ψ_f is the rock-mass or fracture dilation angle. Constant c can be determined from

$$c=\frac{-1\pm\sqrt{1+4a\sigma_{nr}\sqrt{\frac{\phi_{fr}}{12k_{fr}}}}}{2\sigma_{nr}} \quad (2)$$

where σ_{nr} is the reference normal stress, and constant a is assumed to be the reciprocal of the initial normal stiffness (Bandis, et al., 1983). In this study, the normal stress and the fracture permeability and porosity before heating were used as reference. The reference fracture permeability and porosity for Tptpul were 5.50×10^{-13} m^2 and 0.0066, for Tptpmn 2.76×10^{-13} m^2 and 0.01, and for Tptpll 1.29×10^{-12} m^2 and 0.011 (CRWMS M&O, 2001). The initial fracture stiffness was 2.01×10^5 MPa/m (CRWMS M&O, 1999).

As a part of the heater tests, several hydrologic holes were drilled and pressure sensors installed in the holes to measure permeability variations during the heating process. In this paper, the estimated permeability variations at the pressure sensor locations in Holes 57 and 59, at the cross section 10 m from the thermal bulkhead, and Holes 74 and 76, at the cross section 30 m from the thermal bulkhead (Figure 8), were compared with the measured data. Figures 9 and 10 show the variations of permeability as a function of time for Holes 57 and 59 along with field measurements. Letters E and M in the legends denote estimated results and measured data. Vertical axes in the figures are the ratio of the current permeability to the reference permeability. In general, the trends of permeability response to heating for the models with different RMQs and failure criteria were similar. The difference among the models studied was mainly the magnitude of variation.

Figures 9 and 10 suggested that the continuum analyses modeled reasonably the trending of permeability responses to the heating process although there were obvious discrepancies between the estimated and the measured trends. One discrepancy was the variations in permeability estimated at the location of Pressure Sensor 1 (PS1) in Holes 57 and 59. The measured data at this location indicated a permeability reduction (smaller than the reference permeability) trend for the heating duration, whereas the estimated trend was a permeability enhancement (larger than the refer-

ence permeability) at the beginning of the heating. The extent of the enhancement decreased as heating proceeded and, for some models analyzed, this enhancement disappeared and, eventually, led to a permeability reduction. The estimated reduction, however, was small in magnitude when it is compared with the measurements. Also, the measured data and modeling results of all models showed different trending in permeability variations at PS1 in Hole 59.

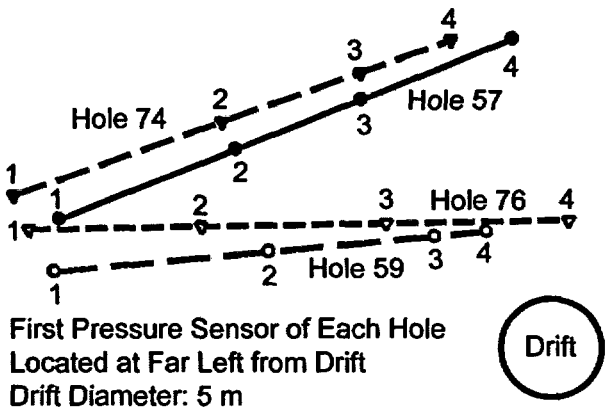

Figure 8. Location of hydrologic holes.

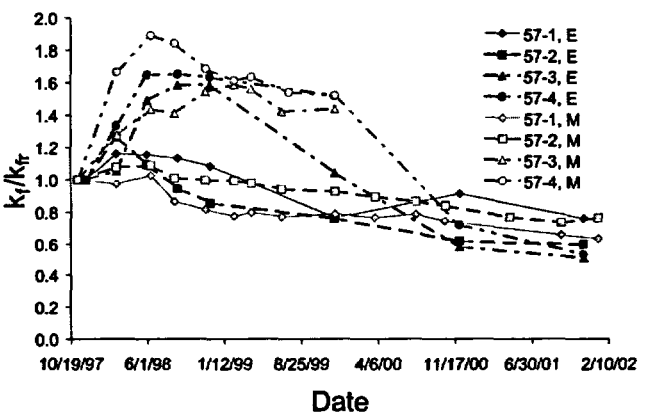

Figure 9. Permeability variations for Hole 57.

The measured data showed permeability recovery at some pressure sensor locations in the middle of the heating process after some large reduction of permeability earlier in the heating process. These pressure sensor locations included PS2 and PS3 in Hole 59 (Figure 10) and PS3 and PS4 in Hole 76 (no figure shown). The permeability at PS3 in Hole 59 not only recovered completely but also started to experience a permeability enhancement between 3 and 4 years of heating. There were two possibilities causing permeability to recover. One possibility was a decrease in fracture normal stress that resulted in a reduction in fracture closure, which, in turn, increased the fracture aperture. When the fracture normal stress became smaller than the reference fracture normal stress, permeability enhancement would result. The other possibility was related to dilation induced by fracture shear displacement. None of the permeability recovery behaviors measured were observed from the modeling results. Unable to predict the recovery behavior limits somewhat the utility of the proposed deformation-permeability relationship. Despite these difficulties, however, the proposed deformation-permeability relationship appears promising for investigating thermal-mechanical effects on rock-mass permeability using a continuum approach. Further studies are needed to identify the sources of the difficulties so that the deformation-permeability relationship can be calibrated, if necessary.

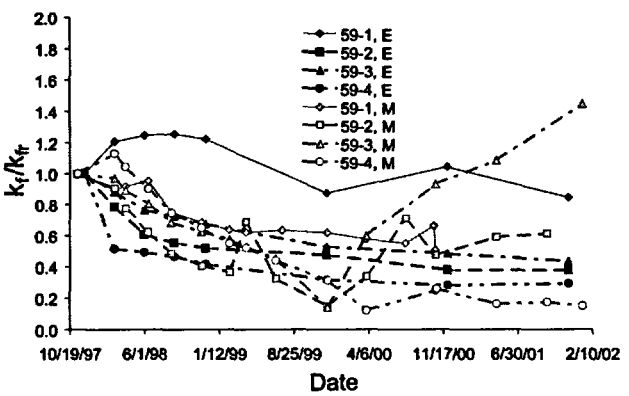

Figure 10. Permeability variations for Hole 59.

Spatial Permeability Variations

Spatial permeability variations in the region 60 m from all sides of the heated drift after 4 years of heating are shown in Figure 11 for the model with the RMQ 2 rock-mass properties and ubiquitous failure criterion. The contours in the figure are ratios of the current permeability to the reference permeability. The figure indicated, in general, a permeability reduction zone surrounding the heated drift regardless of the failure criteria used. This zone extended diagonally outward from the top-left and low-right corners of the heated drift. In this permeability reduction zone, the region with the extensive permeability reduction was in the rock mass immediately surrounding the heated drift. Notice the presence of zones with high permeability enhancement. Locations of these high-

permeability enhancement zones were consistent with those of the shear bands shown in Figure 3(b) [Note the scale difference between Figure 3(b) and Figure 11.]. Notice also the presence of isolated permeability enhancement zones in the essentially permeability reduction zone.

If the same failure criterion was used, the spatial permeability pattern would be the same regardless which rock-mass properties were used. The magnitude of change, however, would be different. In general, the larger the RMQ designations, the greater the variation magnitude.

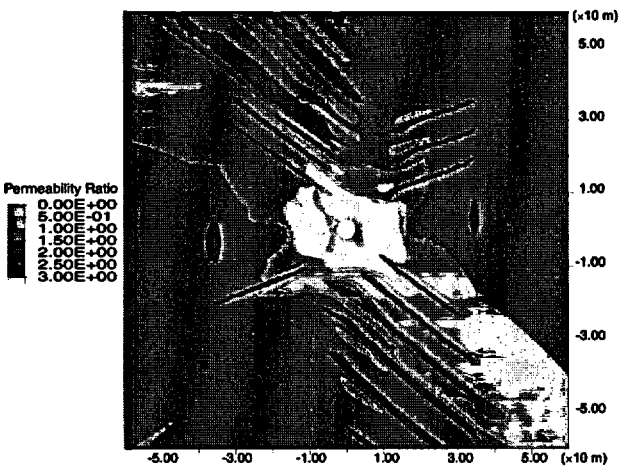

Figure 11. Permeability contour plot for a model using the ubiquitous failure criterion.

4. CONCLUSION

A continuum approach was adopted to assess thermally induced rock-mass responses of a drift-scale heater test. The modeling results underestimated the displacements of the rock mass surrounding the heated drift. One possible cause for the underestimation might be related to the temperature data used. This temperature data set was constructed using a kriging procedure that had the tendency to introduce uncertainties by smoothing out the temperature distribution. These uncertainties could affect the displacement estimation around the heated drift if the temperature in the area was underestimated. Another possible cause might be that the seven heating times used in the analyses were too coarse. For all models studied, large yield zones were developed in the rock mass. Because plastic deformation is path dependent, it may be necessary to use a smaller heating timestep to simulate more realistically the plastic deformation behavior in the analyses.

A normal stress-based deformation-permeability relationship was proposed to investigate the thermal-mechanical effects on rock-mass permeability. The estimated trend of permeability responses to heating compared reasonably to that measured. The modeling results, however, were not able to predict the permeability recovery observed at certain locations.

REFERENCES

Bandis, S.C., A.C. Lumsden, and N.R. Barton. 1983. Fundamentals of Rock Joint Deformation. *International Journal of Rock Mechanics and Mining Sciences & Geomechanics Abstracts.* Vol. 20, No. 6. pp. 249–368.

CRWMS M&O. 2001. *Multiscale Thermohydrologic Model.* ANL–EBS–MD–000049. Rev. 00 ICN 02. Las Vegas, Nevada: CRWMS M&O.

CRWMS M&O. 2000. *Ground Control for Emplacement Drifts for SR.* ANL–EBS–GE–000002. Rev. 00. Las Vegas, Nevada: CRWMS M&O.

CRWMS M&O. 1999. *TBV-332/TBD-325 Resolution Analysis: Geotechnical Rock Properties.* B00000000–01717–5705–00134. Rev. 00. Las Vegas, CRWMS M&O.

CRWMS M&O. 1997. *Ambient Characterization of the Drift-Scale Test Block.* BADD00000–01717–5705–00001. Rev. 01. Las Vegas, Nevada: CRWMS M&O.

Itasca Consulting Group, Inc. 2000. *FLAC—Fast Lagrangian Analysis of Continua.* Version 4.0. Minneapolis, Minnesota: Itasca Consulting Group, Inc.

ACKNOLEDGEMENTS

The work described in the paper was performed at the Center for Nuclear Regulatory Analyses, Southwest Research Institute®, San Antonio, Texas, U.S.A., on behalf of the U.S. Nuclear Regulatory Commission (NRC) Office of Material Safety and Safeguards, Division of Waste Management. This paper is an independent product of the CNWRA and does not necessarily reflect the views or regulatory position of the NRC. The NRC staff views expressed herein are preliminary and do not constitute a final judgment of the matter addressed or of the acceptability of a license application for a geologic repository at Yucca Mountain.